Research Article Vol. 57, No. 28 / 1 October 2018 / Applied Optics 8125

Multiple off-axis fiber Bragg gratings for 3D shape sensing

Christian Waltermann,[1,2,*] Konrad Bethmann,[3] Alexander Doering,[2] Yi Jiang,[3] Anna Lena Baumann,[2] Martin Angelmahr,[2] and Wolfgang Schade[2,3]

[1]FiSens GmbH, Rebenring 33, 38106 Braunschweig, Germany
[2]Fraunhofer Heinrich Hertz Institute, Am Stollen 19H, 38640 Goslar, Germany
[3]Clausthal University of Technology, IEPT, Am Stollen 19B, 38640 Goslar, Germany
*Corresponding author: c.waltermann@fisens.de

Received 15 June 2018; revised 26 August 2018; accepted 27 August 2018; posted 27 August 2018 (Doc. ID 335364); published 25 September 2018

Point-by-point femtosecond laser processed fiber Bragg gratings are arranged around the edge of a standard single-mode optical fiber core. The relative amplitudes of at least three such fiber Bragg gratings are utilized to detect the central position of the mode field within the fiber core and calculate the local curvature of the fiber. An analytical approximation is given, and an experimental validation is performed.

OCIS codes: (060.3735) Fiber Bragg gratings; (060.2370) Fiber optics sensors.

https://doi.org/10.1364/AO.57.008125

1. INTRODUCTION

We report on a novel approach to retrieve the local curvature of a standard single-mode optical fiber based on the analysis of relative amplitudes of at least three femtosecond (fs)-laser-written fiber Bragg gratings (FBGs) arranged around the edge of the waveguiding core. An analytical approximation model and an experimental validation of this approach is given. The proposed interrogation scheme based on the analysis of relative light intensities is immune to polarization effects and wavelength shifts caused by temperature or strain. In addition, the wavelength information of the FBGs remains a free parameter for further sensory tasks.

Since the first reports on point-by-point inscription with femtosecond laser pulses of FBGs [1–3] through the coating of standard single-mode optical fibers it is known that the area of index modification can be of the order of 1 μm^3—small enough to realize several spatially separate gratings at the same position within the core of a typical single-mode fiber. Compared to other core edged FBG structures, several fs-laser-inscribed FBGs in the same plane of a single-mode fiber do not have to overlap physically and the resulting FBG signals do not interfere with each other. Moreover, point-by-point written FBGs could be inscribed customized at any place within the fiber. In 2005, Martinez *et al.* took advantage of this and developed a fiber optical bending sensor based on an eccentrically written FBG [4]. However, only the wavelength shift was used for the evaluation and it turned out that only a much smaller wavelength change could be observed than geometrically predicted. Therefore, a high-precise FBG readout unit has to be used. In addition, temperature and polarization effects were not compensated. In 2018 two similar vector bend sensors based on eccentric FBGs applying a depressed cladding fiber [5] and a multicladding fiber [6], respectively, were presented. In the last-mentioned work, in addition to wavelength information, the intensity information of the created cladding modes of the FBG was also taken into account. Nonetheless, only a single and one-dimensional bending plane was realized.

In more recent years, fiber optical shape sensing based on FBG technology and the resulting applications [7,8] has been a widely discussed and promising field of research. However, to date most approaches turn out to be either too expensive for industrial application (e.g., the inscription and interrogation of FBGs or the analysis of Rayleigh scattering in special multicore fibers that always demand a special fan-out device to address each core separately) or do not allow a high enough number of local curvature sensors for a sufficiently precise shape reconstruction along the entire fiber (e.g., the introduction of additional waveguides to the fiber cladding [9]).

Therefore, a simple solution that allows a great number of curvature sensors within one standard single-mode fiber still has a huge potential for numerous applications in medical or robotic sensing.

Point-by-point fs-laser-inscribed Type II or Type III FBGs (fs FBGs) show a birefringence due to the elliptical shape and locally strong refractive index change at each point of the grating [10]. For orthogonal polarization states this leads to a change of the reflected FBG wavelength of the order of 40 μm/m [11]. In the field of fiber optical shape sensing this effect cannot be neglected since most light sources used for FBG interrogation (like tunable diode lasers or superluminescent diodes) are polarized.

Certain applications (e.g., the navigation of medical catheters within the human body) cannot be realized with such a high uncertainty.

To overcome these drawbacks, we suggest using the relative amplitudes of at least three different point-by-point fs-laser-written FBGs arranged off-center around the fiber core to detect the relative position of the mode field within the core. In comparison to other recent research that utilized basically the same curvature-induced mode field deformation together with a special core dip fiber to create an accelerometer [12], only standard single-mode fiber without any preprocessing or postprocessing is necessary.

In principle three FBGs localized around the outer edge of the fiber core (we will refer to this kind of FBG as "edge FBG," all three together forming an "edge sensor") might also show a curvature-dependent wavelength shift [13]. But the minimal distance to the center of the fiber core and the neutral axis of the curvature, respectively, will lead to very small changes of the Bragg wavelength. In fact, our experiments showed that the bending of FBGs at all possible positions relative to the fiber core leads to much smaller (more than one order of magnitude) wavelength shifts than geometrically expected if only their relative positions to the neutral axis are taken into account. This observation is in accordance to prior results of Martinez *et al.* [4]. Therefore, a reliable bending measurement remains extremely challenging even with most sophisticated interrogation systems available [14,15].

We will demonstrate that a curved fiber induces a polarization-independent change of the backreflected relative light intensities between at least three FBGs arranged around the core of a standard single-mode fiber that can effectively be utilized to retrieve the local curvature.

2. FEMTOSECOND-LASER-INSCRIBED ECCENTRIC CORE EDGE FBG

A. Concept of Relative Amplitude Comparison

The volume of refractive index modification of a typical point-by-point fs FBG can be estimated to 1 μm^3 [16], which is much smaller than the diameter of the entire fiber core (9 μm for SM1550 and 5.8 μm for SM800, the latter of which is used in this work). Due to this, multiple point-by-point fs FBGs can be written side by side into the same fiber core plane.

The mode field intensity within the fiber will be slightly shifted if the glass fiber is curved. Consequently, the coupling between the mode field and an edge FBG will be influenced and the backreflected light of the edge FBG will change. With an edge FBG sensor pattern shown in Fig. 1(a), the position of the mode field or the curvature of the glass fiber, respectively, can be determined by monitoring the intensities of the backreflected light. As example, the intensity changes of two opposite positioned edge FBGs is shown in Fig. 1(b).

If this approach is applied in two dimensions every possible local curvature of the fiber leads to a defined set of edge FBG amplitudes. We will show that it is sufficient to inscribe three edge FBGs at arbitrary different positions around the edge of the fiber core to obtain the two-dimensional curvature information.

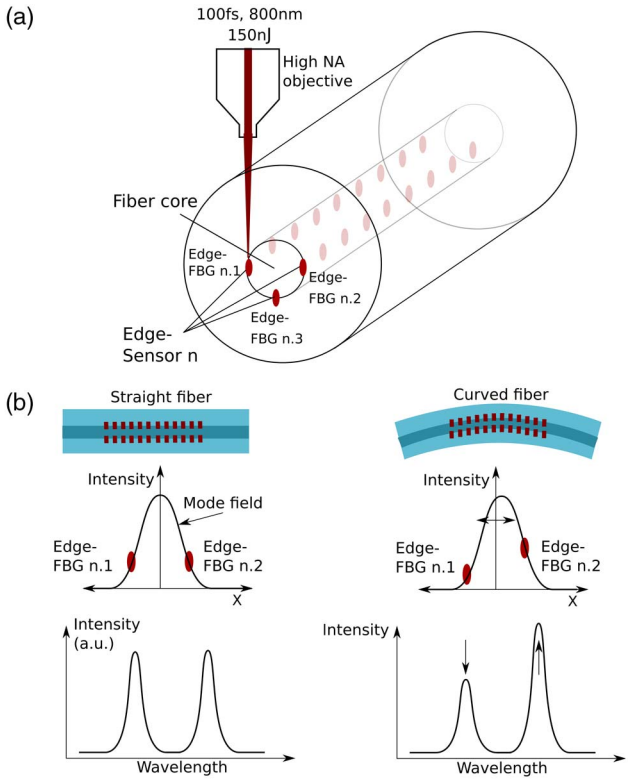

Fig. 1. (a) Point-by-point inscription of three edge core FBGs placed eccentrically around the core of a single-mode fiber forming an "edge sensor." (b) Principle of amplitude-based curvature sensing. Each edge FBG's reflectivity varies with the change of the central position of the mode field.

B. Experimental Setup

A commercial regenerative Ti:Sa amplifier system is used to create laser pulses at 800 nm with an energy of approximately 150 nJ and 100 fs duration. They are focused within the fiber applying a high-NA objective (40×, 0.65NA) to a spot size of less than 1 μm. By shifting xyz-nano-positioning stages, the edge FBGs are inscripted by the point-by-point FBG processing method described in [3] in detail. All three edge FBGs are written with the same processing parameters after each other. In this paper a single-mode fiber for 830 nm has been applied (Fibercore SM800(5.6/125) with an NA of 0.10 and a cut-off wavelength of 690 nm), but all following results could be obtained in the 1.3 μm and 1.5 μm wavelength domains as well. With respect to the center of the fiber core, three edge FBGs are centered at the coordinates (−2.0 μm; 0.0 μm), (+2.0 μm; 0.0 μm), and (0.0 μm; −2.0 μm). A typical spectrum of an array of three such triplets is shown in Fig. 2.

In the given example the edge sensors (each consisting of three edge FBGs) are separated by 2 cm from each other along the fiber.

For each edge FBG triplet, the FBG with the smallest wavelength has the highest reflectivity due to a small constant offset in the applied auto-positioning system or an inhomogeneous focal spot of the fs laser. The processing order of the three FBGs forming each edge sensor has no effect on the resulting relative amplitudes.

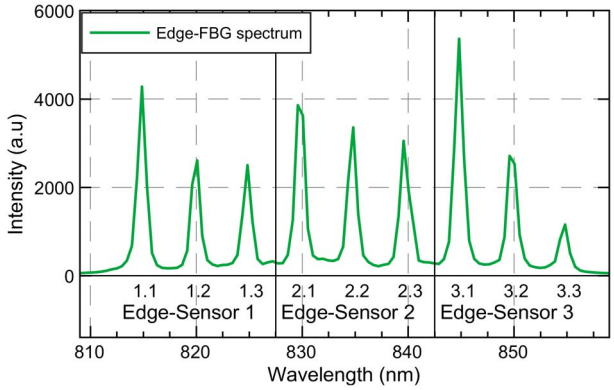

Fig. 2. Spectrum of three edge FBG triplets. Each triplet builds up a curvature sensor plane.

However, to minimize typical transmission losses the edge sensor with the three highest wavelengths is processed with the biggest distance to the interrogation system so there is no light scattering at FBGs that are hit by the light before the target FBG.

Since we will show that only the relative amplitudes are relevant to measure the local curvature of the fiber, moderately different reflectivities have no negative effect on the sensing characteristics. All following experiments have been performed with edge sensor 2 defined by the edge FBG triplet 2.1, 2.2, and 2.3, as shown in Fig. 2.

Figure 3 shows a microscopic image of the fiber core after the processing. All three gratings are clearly visible, and the focal plane of the microscopic camera has been chosen equal to the middle of the fiber core. The edge FBGs have been processed in second order at a wavelength of 800 nm (approximately 590 nm point-to-point distance) with a length of 0.5 mm. This together with the laser spot size means that the grating points are overlapping, but each region with a significant index refraction change is small enough for the grating to take effect. The microscopic image, however, does not reveal any singular points of the gratings, but rather shows three waveguide-like structures instead.

C. Birefringence and Polarization Dependency

It is known that the inscription of Type II FBG with fs laser pulses leads to a certain local birefringence within the fiber and therefore polarization-dependent wavelength and amplitude shift of the FBG [17]. One of the central advantages of a reflectivity-based interrogation of fs-laser-written edge FBGs

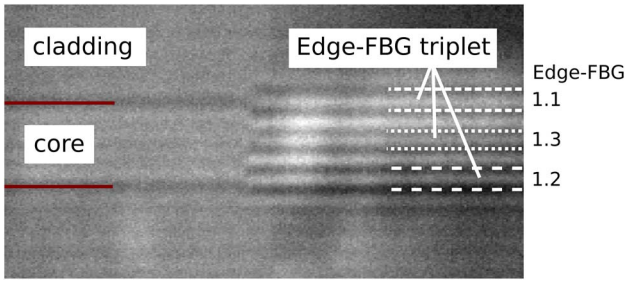

Fig. 3. Microscopic image of an edge FBG triplet.

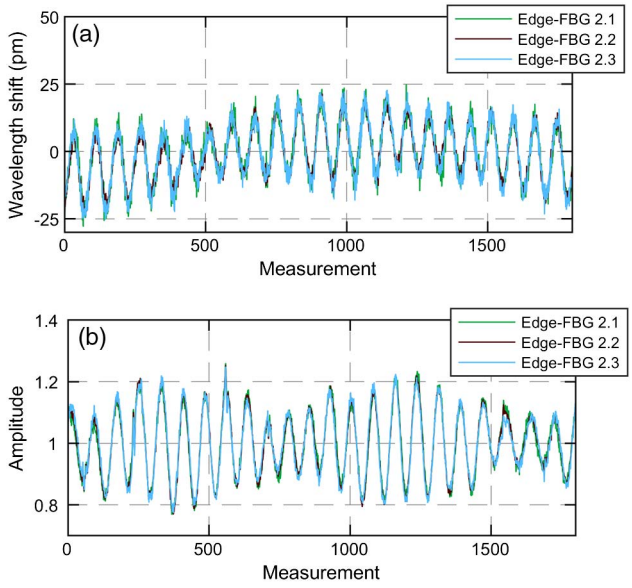

Fig. 4. (a) Polarization-dependent wavelength shift of edge FBGs. (b) Amplitude change.

is that all three gratings will show the same polarization dependency and the relative amplitudes between them remain unchanged. Only the combined birefringence at each position of the waveguide is taken into account.

For proof the presented array of edge FBGs have been interrogated with a polarized light source connected to a slow rotating quarter-wave and a faster rotating half-wave plate applying a high-speed spectrometer (BWTEK Exemplar). This enables an illumination of the edge FBGs with all possible polarization states.

Figure 4(a) shows a characteristic polarization dependency of all three gratings of max ±20 pm. Compared to other reported values this is quite low and shows a good quality of the utilized point-by-point FBG inscription setup. The three edge core gratings clearly show an identical behavior for each applied polarization state. The same occurs to be true for the normalized amplitudes of the three edge FBG, as shown in Fig. 4(b).

Figure 5 depicts the relative changes between the three amplitudes. The systematic patterns nearly vanish, and the overall changes are below 3% of the amplitude, probably caused by spectral underground added to the FBG signal by undesired backscattering of a connector or the end of the sensing fiber. In the chosen visualization a constant offset to all three signals is

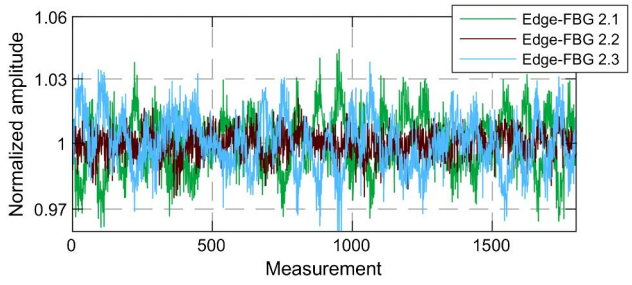

Fig. 5. Relative amplitude change of an edge FBG.

not compensated and could lead to the remaining small systematic differences of the relative amplitudes. Still, the quotient of two edge FBG amplitudes show very little effect due to polarization changes within the fiber.

3. THEORETICAL MODE FIELD DISPLACEMENT AND MATHEMATICAL APPROXIMATION OF RELATIVE EDGE FBG AMPLITUDES

The following section of this paper focuses on the actual behavior of a mode field within a curved single-mode fiber to achieve a quantitative model for the qualitative observations previously described. The mode field within the applied fiber is simulated and its dislocation and deformation due to bending is analyzed. As an approximation an antiproportional shift of a static Gaussian intensity distribution is applied and compared to the simulated light field. This estimation allows us to describe the mode field displacement for all bending radii with a simple analytical solution to derive the actual bending radius from the relative intensity changes of at least three edge FBGs.

A. Mode Field Dislocation in a Curved Single-Mode Waveguide

The simplest approach to mathematically describe the mode field of a single-mode fiber is a Gaussian distribution with the wavelength-dependent diameter ω_m.

For standard single-mode fibers an optimized empiric solution has been given recently in [18]:

$$\omega_m = a\left(172.04e^{\frac{-(V+3.412)^2}{2.141^2}} + 1\right), \tag{1}$$

with the radius of the waveguide a and the normalized frequency V. V can be calculated with the applied wavelength λ, the radius of the waveguide a, and the numerical aperture NA of the fiber used [18]:

$$V = \frac{2\pi}{\lambda} a\mathrm{NA}. \tag{2}$$

The simplest approach of predicting the change in intensity distribution within a curved waveguide would be an antiproportional shift of a constant Gaussian mode field. To evaluate whether the accuracy of this approximation leads to sufficient results the actual electromagnetic field within a bent single-mode fiber has been simulated. A commercial software (PhotonDesign FIMMWAVE) was applied to simulate a straight and several curved waveguides (with bending radii R between 2.1 mm and 500.0 mm) with $a = 2.9$ μm and a numerical aperture NA = 0.10 to the surrounding cladding. This resembles the commercial SM800 single-mode fiber used for all experiments presented in this paper.

In this scenario 2.1 mm radius appeared to be the smallest possible radius that still supports waveguiding. In Fig. 6 the expected difference between the straight fiber (left) and the simulation for the strongest curvature (right) is shown. The position of the maximum intensity changes according to the simulated curvature almost 1.5 μm to the right side and a certain deformation of the intensity pattern can be observed.

For a straight waveguide the simulated intensity distribution overlaps with a Gaussian function with the empirical predicted mode field diameter very well. But for the strongest curvature

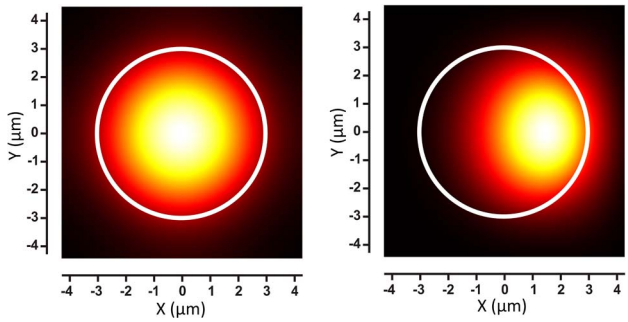

Fig. 6. Simulated mode field for a straight single-mode waveguide for 850 nm and within a curved fiber with a bending radius $R = 2.1$ mm.

the simulation shows a significant asymmetric deformation (Fig. 7).

To analyze the systematical error a linear shifting Gaussian approximation would imply for sensor signals, the local intensities at defined positions have been compared to the more accurate simulated intensity distribution. These localized intensities resemble detectable spectral amplitudes of the edge FBGs written at those positions.

For each simulated curvature with radius R the quotient of two approximated normalized intensities ($I_{\mathrm{FBG1,2}}$) can be calculated as a function of the two distances with respect to the fiber core ($r_{\mathrm{FBG1,2}}$). A simple constant D is introduced to translate the mode field shift of the Gaussian approximation to the radius of the corresponding simulation ($\Delta r = D/R$):

$$I_{\mathrm{FBG1,2}} = e^{\frac{-(r_{\mathrm{FBG1,2}} - \Delta r)^2}{2\omega_m^2}}. \tag{3}$$

For this example ($\omega_m = 1.743$, $D = 354.2$ nm^2, and $r_{\mathrm{FBG1,2}} = \pm 2$ μm), the difference between the simulated data and the Gaussian approximation leads to an error of the resulting curvature below 0.1% of the applied radius for all radii bigger than 10 mm. As shown in Fig. 8(b) even for a 5 mm radius the difference between the simulated and the calculated relative intensities remains well below 1%. An extremely curved fiber with a diameter of 4 mm suffers strong transmission losses, and

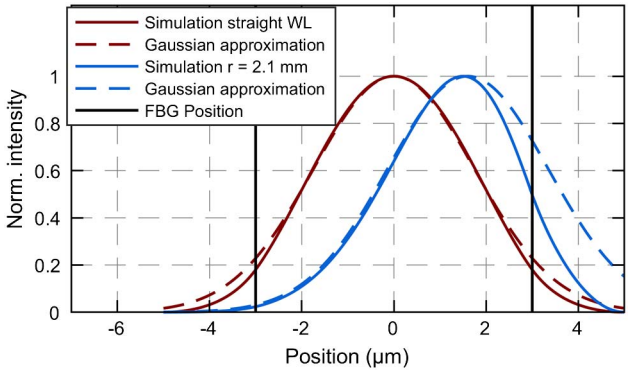

Fig. 7. 1D intensity distribution compared to a Gaussian distribution (straight fiber and curve with $R = 2.1$ mm). In addition to the dislocation of the maximum a deformation occurs.

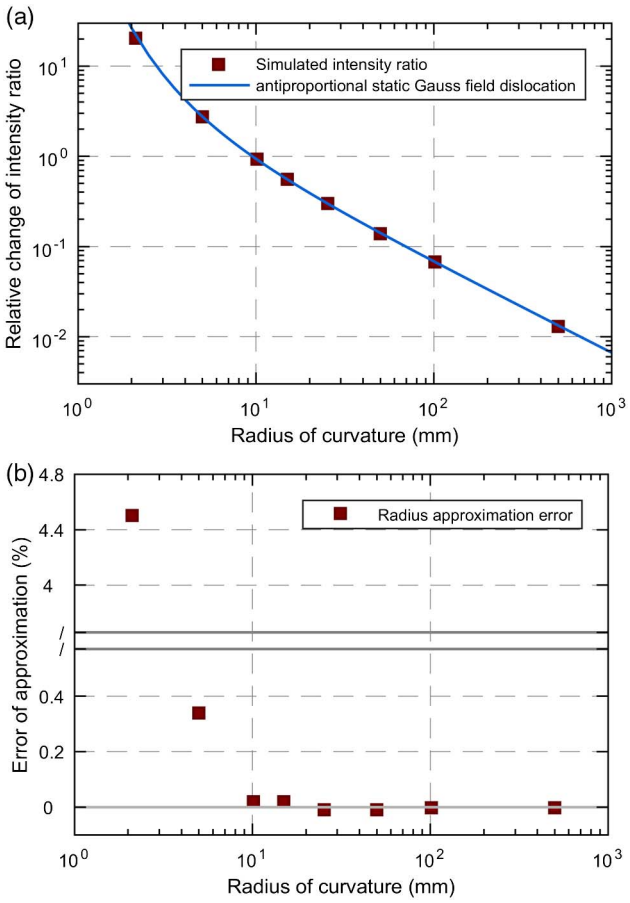

Fig. 8. (a) Simulated change of intensity ratio for two edge FBGs at +2 µm and −2 µm and the corresponding Gaussian approximation. (b) Relative radius error between simulation and approximation.

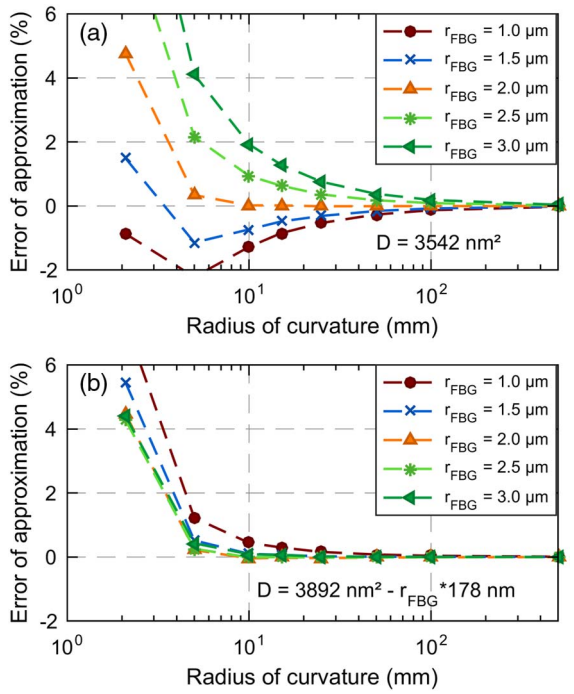

Fig. 9. (a) Relative radius error between simulation and approximation for an edge FBG at different positions with a constant factor D. (b) D as linear function of the distance r_{FBG}.

even in this extreme case the systematic error due to the approximation remains moderately low (4.6%).

If other positions for $r_{\mathrm{FBG1,2}}$ are applied, the difference between both intensities will increase slightly. However, Fig. 9(a) shows that for a reasonable change of the grating distance between 1 µm and 3 µm with respect to the fiber core, the approximation error maintains below 1% of the applied curvature for radii >10 mm. The positioning accuracy of typical commercial xyz-nano-positioning systems is much better than 1 µm and therefore D can be assumed as constant.

For very tight curvatures the position of each grating changes this proportional factor and could be developed as a linear function dependent on the distance r_{FBG} [in this example $D(r_{\mathrm{FBG}}) = 3892\ \mathrm{nm}^2 - r_{\mathrm{FBG}} * 175\ \mathrm{nm}$, Fig. 9(b)].

Consequently, for first experimental applications the proposed approximation of a static Gaussian mode field that shifts antiproportional to the curvature is sufficient to retrieve the bending information with an uncertainty below 1%.

B. Analytical 2D Curvature Calculation with Three Edge FBGs

Obviously, it is the biggest advantage of a Gaussian approximation that an analytical solution can be found for all parameters within the equation. The following calculations have been performed in Cartesian coordinates and therefore the perpendicular mode field shifts Δx and Δy are the desired unknown values. They are dependent on the detected backreflected FBG intensities at the coordinates around the fiber core. Additionally, the global light intensity within the fiber I_{Global} is typically unknown and therefore it is necessary to analyze at least three edge FBGs at different positions to solve the equations and retrieve all three parameters.

Within the symmetric Gaussian approximation, the backreflected intensity of each edge FBG (I_{1-3}), depending on its position (x_{1-3}, y_{1-3}) and the displacement of the mode field $(\Delta x, \Delta y)$, can be written for each edge FBG as

$$I_{1-3} = I_{\mathrm{Global}} e^{\frac{-((x_{1-3}-\Delta x)^2+(y_{1-3}-\Delta y)^2)}{2\omega_{\mathrm{m}}^2}}. \tag{4}$$

Together with the mode field diameter ω_{m} three of these equations with different values for the position x_{1-3} and y_{1-3} can be derived to

$$\Delta y = \frac{A_{1,2} - A_{2,3}}{C_{1,2} - C_{2,3}} \tag{5a}$$

and

$$\Delta x = A_{1,2} + C_{1,2}\Delta y, \tag{5b}$$

with

$$A_{i,j} = \frac{2\omega_{\mathrm{m}}^2 \ln\left(\frac{I_i}{I_j}\right) + x_i^2 + y_i^2 - x_j^2 - y_j^2}{2(x_i - x_j)} \tag{6a}$$

and

$$C_{i,j} = \frac{y_j - y_i}{x_i - x_j}. \tag{6b}$$

Therefore, the change of the mode field position can be calculated with the knowledge of three edge FBG positions with respect to the fiber core and their current intensity. Global changes to the light intensity guided within the fiber (I_{Global}) have no effect on the resulting mode field shift.

As shown in the previous section the radius of curvature can be estimated as antiproportional to the displacement of the mode field with the fiber-dependent constant D that can be retrieved from the simulation above and equals in this case approximately $D = 354.2\ \mathrm{nm}^2$. Transformed to polar coordinates the direction (φ) and the bending radius (R) can be obtained:

$$R = \frac{D}{\sqrt{\Delta x^2 + \Delta y^2}} \varphi = \tan_2^{-1}(\Delta x, \Delta y). \tag{7}$$

In summary, the relative intensities of three edge FBGs inscribed in a fiber at arbitrary positions with respect to the fiber core are sufficient to retrieve an analytical localization of the mode field within the fiber. In turn this position shifts antiproportional with the applied radius of curvature. Since only the quotient of the normalized intensities is considered, all global changes to the backreflected intensity have no effect on the result. This makes the edge FBG a very robust and promising approach to detect curvatures.

4. EXPERIMENTAL VALIDATION AND CURVATURE SENSING

In this section we apply the analytical approximation given above to real edge FBG fibers and validate the experimental capability of this approach. The sensors signals are monitored while bent in all directions at several defined reference curvatures. The resulting amplitude change and phase of each edge FBG is used to calibrate the actual positions of the fs-laser-inscribed structure.

A. Reference Curvatures

To allow an experimental validation of the calculations above, several fiber guidance tools with defined reference curvatures have been manufactured. As shown in Fig. 10, the edge FBG fiber is inserted into defined circular paths with different radii. While the fiber maintains fixed in its position, the tool is rotated around the entrance point of the sensor with a stepper motor. The edge FBGs are positioned in the middle of the rotating curvature.

For each step the amplitudes of three edge FBGs that form a sensor plane are recorded with a commercial microspectrometer (Ocean Optics STS). A simple Gaussian peak fit has been applied, which is also useful to obtain the edge FBG wavelength at the same time. Of course, other known peak detection algorithms can be applied as well.

During the processing of an actual edge FBG fiber it is not possible to guarantee that each processed FBG has the same absolute intensity. Therefore, each sensor signal (I_{RawFBG} with FBG = 1–3) must be normalized with an additional constant (N_{FBG}) to obtain a comparable triplet of intensities (I_{FBG}) for each sensor plane:

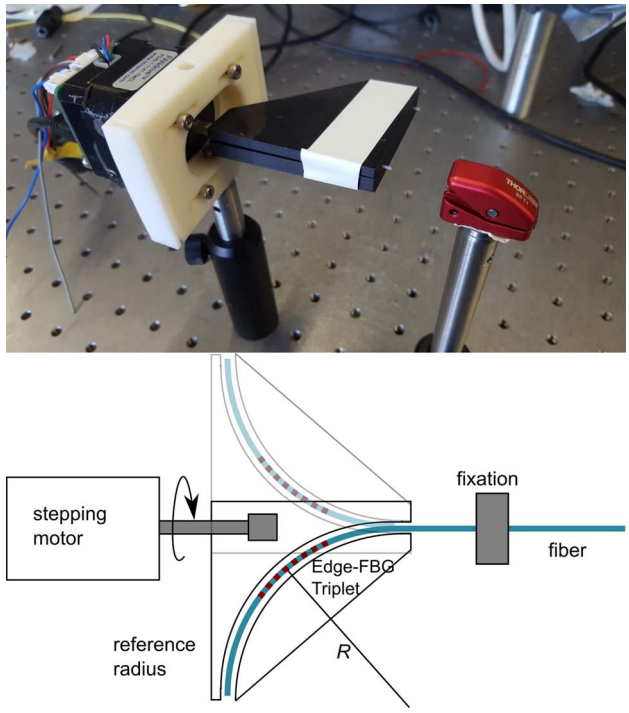

Fig. 10. Photo and schematic of the experimental validation setup. An edge FBG fiber is guided within a guidance tool with a defined radius that can be rotated to bend the sensor in all directions.

$$I_{\mathrm{FBG}} = \frac{I_{\mathrm{RawFBG}}}{N_{\mathrm{FBG}}} \tag{8}$$

This parameter corrects the measured amplitudes of a straight fiber to the theoretical relative intensities of a one-dimensional Gaussian distribution at the distance to the center of the fiber core (r_{FBG}), e.g., approximately to 0.5 in the given example. This can easily be done by measuring the amplitudes of a straight fiber ($I_{\mathrm{StraightFBG}}$):

$$N_{\mathrm{FBG}} = I_{\mathrm{StraightFBG}} / e^{\frac{-r_{\mathrm{FBG}}^2}{2\omega_{\mathrm{m}}^2}}. \tag{9}$$

Both position and spectral response of the gratings will remain constant after processing. Changes to the applied light intensity will not affect this normalization since all three edge FBGs behave symmetrically.

Figure 11 depicts the normalized intensities of an edge FBG triplet rotated around a reference curvature with $R = 20$ mm.

The sensor analyzed in Fig. 8 has been designed with a perpendicular geometry and an identical distance between each edge FBG and the fiber core (2 μm). Therefore, the amplitude of all three oscillations can be expected to be equal and their phases also identical 90° to each other. If the assumed processing positions are used to calculate the mode field shift according to Eqs. (5a) and (5b), Δx and Δy appear (in this case for a radius of 20 mm) 10% to 20% bigger than the value of the reference radius and follow an elliptical shape, as illustrated in Fig. 12.

The processing stability of the true central position of each edge FBG is limited due to the mechanical stability of the nanopositioning system. Additionally, the curved surface of the fiber

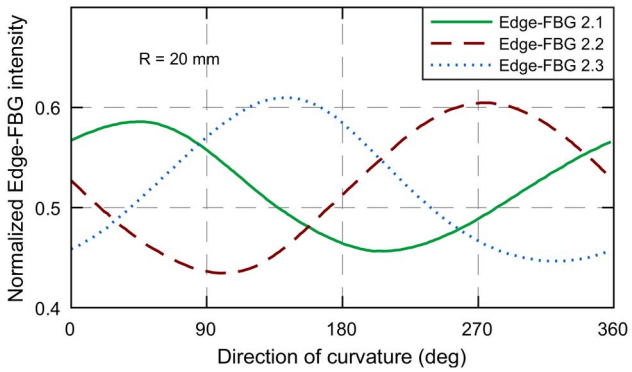

Fig. 11. Normalized amplitude of three edge core FBGs.

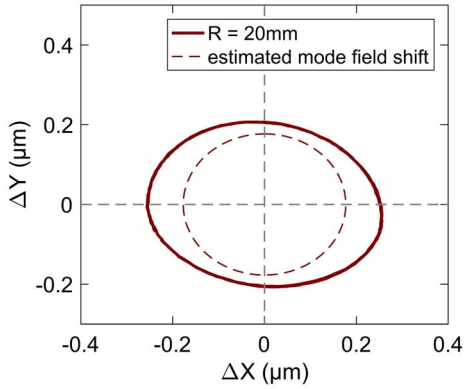

Fig. 12. Reconstructed mode field displacement for an uncalibrated edge FBG sensor with assumed edge FBG positions according to the inscription process.

may lead (even within immersion) to a certain offset between the programmed edge FBG position and the real focal spot of the laser.

The better the absolute positioning of each edge FBG during the fs laser inscription process, the smaller the radius sensing error or at least the difference between several edge FBG sensors. However, it is possible to overcome all processing uncertainties with the measurement of one reference curve with a defined radius and calibrate the actual position of each grating.

B. Edge FBG Calibration

According to Eq. (6a) the mode field shift can be approximated as linear to the logarithm of the normalized intensity change. While rotated around a constant radius the absolute value of the shift remains constant, only the direction oscillates with the direction of curvature (α). Therefore, the detected intensity changes according to the exponent of a sinusoidal function and can be approximated as

$$I_{\mathrm{FBG}}(\alpha) = I_{\mathrm{StraightFBG}} + (I_{\max} - I_{\min})e^{\sin(\alpha+\varphi)}. \tag{10}$$

Figure 13 shows a very good overlap between all measured intensities and their curve fits. The experimental data shows a minimal asymmetric deformation compared to the model approximation. The coated fiber used for this experiment is

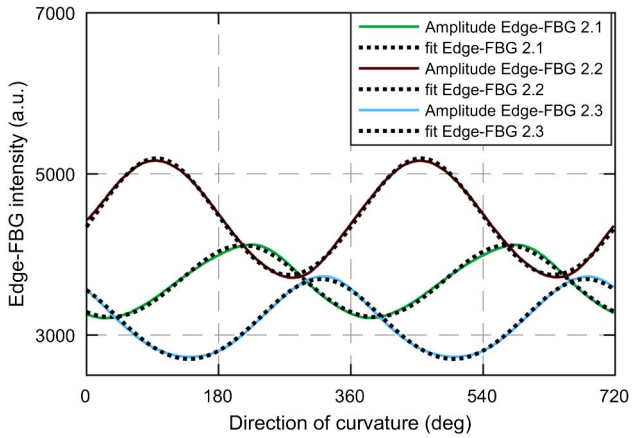

Fig. 13. Curve fit of measured amplitudes of three edge FBGs. Minimal asymmetries are due to a preferred bending direction of the coated fiber.

stored wounded up and shows a slightly preferred bending direction. Within the reference radius, this leads to a small torsion of the fiber to avoid a curvature contrary to this preferred direction.

The fitted values for the maximum and minimum intensity equal the mode field shift for a fiber exactly curved in or inverse to the direction of the edge FBG with respect to the center of the fiber core. For these two cases Eq. (4) can be simplified to one dimension:

$$I_{\max,\min} = N_{\mathrm{FBG}} I_{\mathrm{Global}} e^{\frac{-(r_{\mathrm{FBG}} - \Delta r_{\max,\min})^2}{2\omega_{\mathrm{m}}^2}}. \tag{11}$$

For maximum and minimum intensity, the mode field shifts with the same absolute value (Δr) in opposite directions ($\Delta r_{\min} = -\Delta r_{\max} = \Delta r$). I_{Global} and N_{FBG} maintain unchanged during the reference measurement.

With the empirical constant for the applied fiber D introduced in Section 3.A of this paper ($\Delta r = D/R$) both equations can be solved and lead to the desired true distance between the edge FBG and the center of the fiber core r_{FBG}:

$$r_{\mathrm{FBG}} = \frac{\omega_{\mathrm{m}}^2}{2\Delta r} \ln\left(\frac{I_{\max}}{I_{\min}}\right) = \frac{\omega_{\mathrm{m}}^2 R}{2D} \ln\left(\frac{I_{\max}}{I_{\min}}\right). \tag{12}$$

Combined with the fitted phase φ, the position of each edge FBG and the normalization constant C_{FBG} (with $I_{\mathrm{Global}} = 1$ for the calibrational measurement) can be obtained.

For this example, Fig. 14 depicts the calibrated coordinates of all three edge FBG sensors compared to their desired processing positions. Especially the lower two edge FBGs have repeatedly been processed about 1 μm below the programmed parameters and have a significantly larger distance to the center than expected. Other identically processed sensors show a similar behavior. Therefore, an additional systematic processing error occurs that could be corrected already during the inscription. However, since the demonstrated calibration allows arbitrary edge FBG positions, this offset can be tolerated. All edge FBG coordinates and the constants C_{FBG} remain unchanged for as long as the sensor exists.

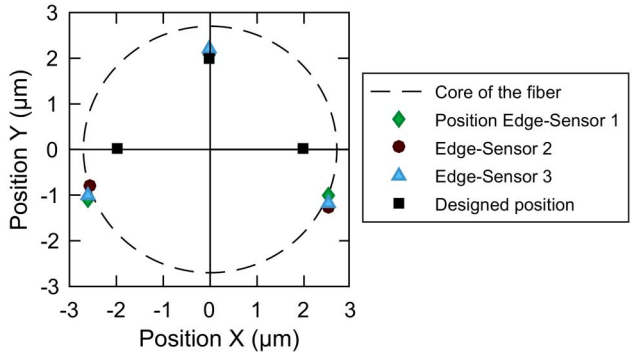

Fig. 14. Calibrated edge FBG positions compared to processed sensor design.

C. Evaluation of Calibrated Edge FBG Sensor

If the calibrated positions of an edge FBG are applied to the reference measurement, the resulting radius of curvature remains closer to the same value as compared to the uncalibrated measurement in Fig. 12. The maximum difference between the applied radius and the measurement is reduced to approximately 2%. In Fig. 15 the calibrated sensor is tested with several other reference radii R between 5 mm and 50 mm.

For the applied curves the sensor shows a very good overlap between measured and expected radius in all possible directions.

For a better quantification, Fig. 16 depicts the average detected radii and the maximum difference for all directions. All measurements provide a very good linearity of the calibrated sensor and a maximum radius error below 8% for the biggest curvatures ($R = 50$ mm $\pm$ 3 mm) and below 4% for radii smaller than 25 mm (e.g., $R = 10$ mm $\pm$ 0.2 mm). The signal-to-noise ratio of the spectrometer measurement leads to a maximum detectable radius of the order of 10 m.

Especially for the correct detection of large radii (and therefore small changes of the edge FBG amplitudes) it is necessary to avoid any backscattering from connectors or the end of the fiber, since those lead to a change of the relative amplitudes. This in turn results in a slightly changed central position of the circles shown in Fig. 15 and therefore an increase in curvature detection error.

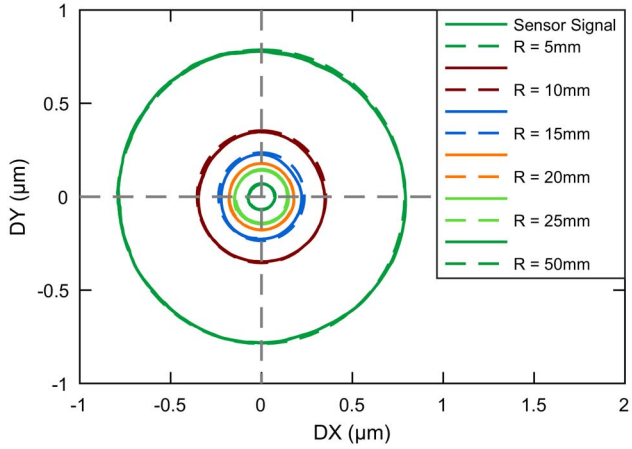

Fig. 15. Calibrated edge FBG triplet: calculated mode field shift during reference measurement (color online).

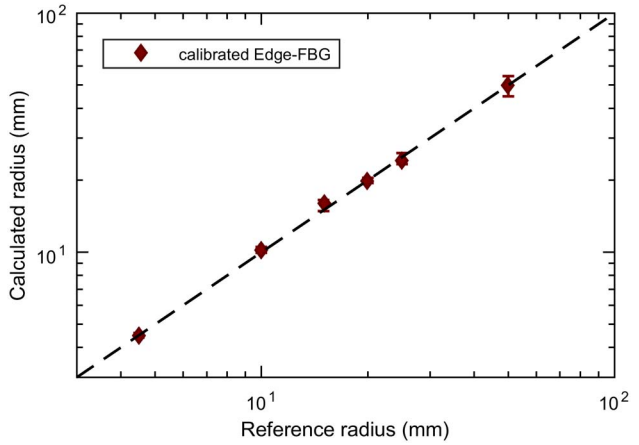

Fig. 16. Calculated radius of curvature for different reference radii. The error resembles the maximum and minimum radius according to the calculation.

In comparison only very small curvature-dependent wavelength shifts have been observed. Even for the smallest radius (5 mm) the maximum difference of the wavelength has only been of the order of 15 pm. The applied simple interrogation system (Micron Optics STS spectrometer, 80 Hz repetition rate and no further averaging) allows a reproducible Bragg wavelength detection of the order of 2 pm or a maximum radius of curvature of a few centimeters. Therefore, with the given setup the shown amplitude-based interrogation of edge FBGs appears to be several orders of magnitude more sensitive than a wavelength interrogation of the identical sensor.

Even with more sophisticated interrogation systems (as mentioned above) it is not likely to overcome this difference completely since a better wavelength detection will improve the amplitude detection as well.

D. Outlook: Time-Domain Standard Single-Mode Optical Fiber Shape Sensing

Multiplexing is a critical point of all proposed variants of fiber optical shape sensing so far. To obtain a precise three-dimensional reconstruction the local curvature information from numerous points along the fiber is required. Spectroscopic FBG interrogation is always limited to the bandwidth of the applied systems. However, since the proposed edge FBG does not change its wavelength due to bending, the spectral distance between two FBGs can be very small and the readout of a large number (up 10–15 curvature sensors) within one fiber is possible.

If even more sensor information points are necessary, time-domain interrogation techniques can be applied [13]. Hundreds of identical FBGs with a very low reflectivity can be analyzed within one single fiber. Backscattering of connectors or the end of the sensor fiber do not affect the reflected intensities and therefore a time-domain interrogation of the edge FBG would improve the sensor's quality and its stability for application. The only requirements are the analyzation of three different wavelength channels according to the

wavelengths of each edge FBG triplet and a sufficient distance between each triplet to allow the separation of the signals. This can be realized with fiber Bragg grating readout units, combining time and wavelength domains [19,19]. Further, the cumulated intensity of all edge FBGs with an identical wavelength should not be bigger than a few percent to minimize the amplitude change of the later edge FBG due to bending of the first sensors. Otherwise, for example, a bending-induced collective increase of the reflectivity of all but the last edge FBG with the same wavelength would lead to a significant change for the remaining intensity for the specific wavelength at the end of the fiber.

5. CONCLUSION

The local curvature of a fiber can be detected by analyzing the intensity amplitude of three femtosecond-laser-written FBGs arranged around the outer edge of a standard single-mode fiber core. An analytical approximation has been proposed and evaluated. For bending radii larger than 5 mm the mode field within a single-mode fiber can be interpreted as a static Gaussian field that shifts its position antiproportional with the bending radius. For a simple detection of the direction of curvature it is sufficient to apply the designed positions of each FBG to the model. For more accurate measurements that are required for 3D shape sensing applications with multiplexed edge FBG sensors, the processing must be extremely precise and reproducible (the laser focus positioning of the order of 20 nm for 800 nm fibers). Alternatively, a triplet of edge FBG can be calibrated with one reference curvature. Even with a simple commercial micro-spectrometer, a calibrated edge FBG triplet is capable of detecting radii between about 10 m and 5 mm for all possible directions with good linearity. More precise interrogation systems with higher signal-to-noise ratios, a higher resolution, and perhaps additional averaging should allow improvement of the sensitivity of curvature sensing at least by 1 or 2 orders of magnitude. However, we do not think that the presented shape sensor is appropriate for the detecting of curvatures of the order of several kilometers, as required for downhole monitoring by the oil and gas industry. It seems much more likely to apply this approach for several medical procedures with the requirement of very small radii and a still significant number of sensor planes. Further, if this approach is performed at 1550 nm, all distances will be approximately twice as big as shown in this paper. Therefore, for applications that do not allow a calibration for every single sensor the average results will improve due to the larger mode field diameter and therefore relatively smaller edge FBG positioning errors compared to the center of the fiber core during the inscription process.

REFERENCES

1. A. Martinez, M. Dubov, I. Khrushchev, and I. Bennion, "Direct writing of fibre Bragg gratings by femtosecond laser," Electron. Lett. **40**, 1170–1172 (2004).
2. A. Martinez, I. Y. Khrushchev, and I. Bennion, "Direct inscription of Bragg gratings in coated fibers by an infrared femtosecond laser," Opt. Lett. **31**, 1603–1605 (2006).
3. J. Canning, M. Stevenson, S. Bandyopadhyay, and K. Cook, "Extreme silica optical fibre gratings," Sensors **8**, 6448–6452 (2008).
4. A. Martinez, Y. Lai, M. Dubov, I. Y. Khrushchev, and I. Bennion, "Vector bending sensors based on fibre Bragg gratings inscribed by infrared femtosecond laser," Electron. Lett. **41**, 472–474 (2005).
5. W. Bao, Q. Rong, F. Chen, and X. Qiao, "All-fiber 3D vector displacement (bending) sensor based on an eccentric FBG," Opt. Express **26**, 8619–8627 (2018).
6. F. Chen, D. Su, X. Qiao, and Q. Rong, "Compact vector bend sensor using dual-off-axis innermost cladding-type FBGs," IEEE Sens. J. **18**, 7476–7480 (2018).
7. G. Allwood, G. Wild, and S. Hinckley, "Fiber Bragg grating sensors for mainstream industrial processes," Electronics **6**, 92 (2017).
8. R. Willsch, W. Ecke, and H. Bartelt, "Optical fiber sensor research and industry in Germany: review and outlook," Proc. SPIE **7753**, 775302 (2011).
9. C. Waltermann, A. Doering, M. Köhring, M. Angelmahr, and W. Schade, "Cladding waveguide gratings in standard single-mode fiber for 3D shape sensing," Opt. Lett. **40**, 3109–3112 (2015).
10. Y. Lai, A. Martinez, I. Khrushchev, and I. Bennion, "Distributed Bragg reflector fiber laser fabricated by femtosecond laser inscription," Opt. Lett. **31**, 1672–1674 (2006).
11. J. Burgmeier, C. Waltermann, G. Flachenecker, and W. Schade, "Point-by-point inscription of phase-shifted fiber Bragg gratings with electro-optic amplitude modulated femtosecond laser pulses," Opt. Lett. **39**, 540–543 (2014).
12. Q. Rong, T. Guo, W. Bao, Z. Shao, G. Peng, and X. Qiao, "Highly sensitive fiber-optic accelerometer by grating inscription in specific core dip fiber," Sci. Rep. **7**, 11856 (2017).
13. C. Waltermann, J. Koch, M. Angelmahr, J. Burgmeier, M. Thiel, and W. Schade, "Fiber optical 3D shape sensing," in *Planar Waveguides and other Confined Geometries*, G. Marowsky, ed., Springer Series in Optical Sciences (2014), Vol. **189**.
14. C. G. Askins, G. A. Miller, and E. J. Friebele, "Bend and twist sensing in a multiple-core optical fiber," in *OFC/NFOEC 2008–2008 Conference on Optical Fiber Communication/National Fiber Optic Engineers Conference* (2008), pp. 1–3.
15. G. A. Miller, C. G. Askins, and G. A. Cranch, "Interferometric interrogation of a multicore fiber, two-axis inclinometer," Proc. SPIE **7503**, 75032R (2009).
16. E. N. Glezer and E. Mazur, "Ultrafast-laser driven micro-explosions in transparent materials," Appl. Phys. Lett. **71**, 882–884 (1997).
17. F. Mitschke, *Fiber Optics: Physics and Technology* (Springer-Verlag, 2010).
18. B. Yang, J. Duan, Z. Xie, and H. Xiao, "Evaluation of mode field diameter of step-index fibers and comparison analysis," Res. J. Appl. Sci. Eng. Technol. **6**, 382–386 (2013).
19. A. Doering, W. Schippers, J. Koch, M. Angelmahr, and W. Schade, "Combined time and wavelength domain interrogation scheme for readout of fiber Bragg grating arrays," in *Proceedings of OSA BGPP*, Zürich (2018).